Direct pickup and knockout processes in inclusive (p,dx) reactions at 42–392 MeV

Yusuke Uozumi,* Yuji Yamaguchi, Gaku Watanabe, Yuki Fukuda, Ryota Imamura, and Monira Jannatul Kobra
Department of Applied Quantum Physics and Nuclear Engineering, Kyushu University, 744 Motooka, Nishi-ku, Fukuoka 819-0395, Japan

Masahiro Nakano
Junshin Gakuen University, 1-1-1 Chikushigaoka, Minami-ku, Fukuoka 815-8510, Japan

(Received 5 January 2018; published 30 March 2018)

Inclusive (p,dx) reactions at 42–392 MeV are investigated to understand quantitatively the roles of direct pickup and knockout. These two processes are formulated and introduced into the intranuclear cascade model. The calculated spectral shapes and magnitudes of the double-differential cross sections agree well with all experimental observations over the entire ranges of emission energy and laboratory angle. The model reveals the contributions of pickup and knockout in terms of incident-energy dependence. Direct pickup accounts for the highest energy domain of the spectra of not only discrete but also continuum regions with excitations up to around 45 MeV. Knockout becomes increasingly important with incident proton energy. It is negligible at 42 MeV, occupies the lower half of spectra at 90 MeV, and above 300 MeV is responsible for most of each energy spectrum except the part at highest energy. This trend is very similar to that of (p,nx) cross sections. The indirect pickup component appears at these energies, as suggested in previous studies.

DOI: 10.1103/PhysRevC.97.034630

I. INTRODUCTION

The purpose of this article is to improve our understanding of inclusive (p,dx) reactions at incident energies of 42–392 MeV. Proton-nucleus reactions are generally well described by the two-step mechanism [1,2]. The first-step processes (which account for most of each double-differential cross-section [DDX] spectrum except the part at lowest energy) in deuteron production reactions come in several competing types according to the proton incident energy. The second step, namely the evaporation process from excited equilibrium states, is beyond the scope of the present study.

Considerable efforts have been made to unravel the exclusive (p,d) reaction mechanisms at incident energies of around 50 MeV (i.e., the medium energy range). Direct pickup or knockout populating low-lying discrete levels is now well understood. However, relatively little attention has been paid to reactions that lead to continua spreading over wide excitation regions. We attempted to interpret (p,dx) DDX spectra by the sum of the first-order distorted-wave Born-approximation (DWBA) cross sections [3–5]. Our calculation results agreed with experimental results in the low-excitation region but underestimated them considerably in the high-excitation region. We attributed this inconsistency at high excitations to a failing of the first-order DWBA: One or more particles may be emitted along with the observed one, and the absorption by the imaginary optical potential is recognized as particle loss. Moreover, the DWBA is inadequate because high-excitation levels are not pure single-hole states and the transitions co-occur with large momentum transfer. In order to avoid these shortcomings, Hashimoto *et al.* [6] applied the DWBA to only low-lying discrete levels, and calculated the high-excitation continuum states by the intranuclear cascade (INC) model: However, this is the case for (d,px) reactions.

Other approaches were based on phenomenological studies of angle-integrated spectra. Kalbach [7,8] proposed an empirical treatment of direct pickup for the low-excitation transitions and ascribed high excitations to pre-equilibrium particle emission, which was calculated with the exciton model [9,10]. Similar approaches were made by Konobeyev *et al.* [11,12]; in Ref. [12], in addition to direct pickup, these included the pickup process from the $2p1h$ exciton state, the coalescence of two excited nucleons above the Fermi energy, and the knockout of a preformed deuteron. The Kalbach approach [7] suggests that the direct-pickup yield covers a wide spectral range, whereas the Konobeyev approach suggests that the same is true for the knockout yield. Machner [13] extended the exciton model to take cluster condensation into account. Hachenberg *et al.* [14] attempted to describe the reactions in terms of indirect pickup only. Although all of them gave rather good accounts of angle-integrated spectra, their interpretations of deuteron production mechanisms are remarkably inconsistent.

At impinging energies higher than 700 MeV, deuteron production has been investigated in terms of knockout [15–18], the direct production of $p + N \rightarrow d + \pi$ [16,18,19], and the indirect process described by the coalescence model [20–26]. Knockout is the process whereby a preformed deuteron inside a target nucleus is knocked out, and a group of such knocked-out deuterons forms a broad peak in the higher energy domain of spectra at forward angles. The center of the peak is shifted 10–20 MeV down from the value of proton-deuteron elastic scattering, and its spread is understood as the Fermi motion. It is notable that no quasifree peak is observed in

*uozumi@nucl.kyushu-u.ac.jp

the medium-energy reactions. The coalescence model was invented by Butler and Pearson [20] and is based on the assumption that any two nucleons that escape the nucleus and whose relative momentum is less than a certain value coalesce to form a deuteron. Note that this coalescence model involves an idea similar to that of Konobeyev but uses different implementations.

At proton bombarding energies of around 400 MeV, deuteron continua have been explained rather successfully in terms of knockout and indirect pickup. The latter [27,28] is pickup by a secondary nucleon scattered via one or more nucleon-nucleon collisions between an incident proton and a target nucleon below the Fermi energy. It was proposed to explain the low-energy spectra of large angles ($>60^\circ$) at a bombarding energy of 300 MeV, which could not be explained by the direct-pickup theory. The measured target-mass dependence of the reaction cross sections supports the indirect process. It has been suggested that this process is negligible below 200 MeV [27] but important at 600 MeV [28].

In our previous work [29], we developed the INC model to include these two processes, and we succeeded in reproducing experimental DDX spectra of (p,dx) reactions at 300 and 392 MeV over nearly the entire energy range including the quasifree bump observed at forward angles on various target nuclei. The remarkable feature of the INC is that it treats two-body collision kinematics exactly, and hence quasifree peaks were shown to come from nucleon-nucleon collision but not nucleon-deuteron elastic scattering. It was shown also that the knockout contribution dominates most of each spectrum, that the indirect pickup appears in the low-energy region just above the evaporation energies, and that the coalescence component is unimportant. This last feature is consistent with Refs. [27,30].

The above context suggests that inclusive (p,dx) reactions in the medium-to-intermediate energy range should be interpreted as direct-pickup and knockout processes. In the present study, we analyze DDX spectra to reveal the roles of the two processes by improving our INC model. Although the INC model had been applied to reactions at incident energies higher than roughly 200 MeV, we extended the model successfully [31,32] to the lower part of the medium-energy range by introducing some physics that had been neglected in previous studies on INC. Therefore, our extended INC model (referred to hereinafter as the EINC model) is fruitful for the present purpose. We have already included direct pickup [33], knockout [29], and indirect pickup [29] in INC. Now we improve the descriptions of direct pickup and knockout to obtain a consistent exposition of (p,dx) reactions at incident energies of 42–392 MeV. We choose ^{27}Al as the target nucleus because DDX data on ^{27}Al could be obtained at five incident energy values, the most available in the energy range of interest.

II. MODEL

A. EINC model

Because the EINC model is detailed fully in Refs. [31,32], we merely outline it herein. The original INC model involves transferring energy to the target nucleus through only a sequence of nucleon-nucleon collisions. When nucleon i approaches nucleon j within a distance equivalent to the nucleon-nucleon cross section σ_{NN} [34], that is,

$$r_{ij} < \sqrt{\frac{\sigma_{NN}}{\pi}} \tag{1}$$

the probability of the two nucleons colliding is judged phenomenologically using the Pauli blocking operator:

$$\hat{Q}|ij\rangle = [1-\Theta(E_i - E_F)][1-\Theta(E_j - E_F)]|ij\rangle, \tag{2}$$

where E_i is the energy of nucleon i after the collision and E_F is the Fermi energy. Θ denotes the unit step function. The scattering angle is determined stochastically to follow angular distributions of NN collisions.

The EINC model includes additional physics that are important for medium-energy reactions. For instance, the proton production DDX by proton incidence is expressed by

$$\left.\frac{d^2\sigma}{dEd\Omega}\right|_{\theta,\varepsilon} = \sigma_{\rm total}\frac{1}{2\pi\Delta E\Delta\cos(\theta)}P^p(\theta,\varepsilon), \tag{3}$$

where ΔE and $\Delta\cos\theta$ are the bin widths of the outgoing energy, ε, and the emission angle, θ, respectively. $\sigma_{\rm total}$ is the proton-nucleus total cross section, which is assumed to be equal to $\pi R_{\rm max}^2$. $R_{\rm max}$ is the maximum nuclear radius in femtometers given by $r_0 + 4a_0$, where $r_0 = (0.976 + 0.0206A^{1/3})A^{1/3}$ and $a_0 = 0.54$. The proton emission probability P^p is written symbolically as

$$P^p(\theta,\varepsilon) = P^p_{\rm def}(1+P_{CE})[\hat{G} + \hat{G}(\hat{Q}P_{NN})\hat{G} + \hat{G}(\hat{Q}P_{NN}) \times \hat{G}(\hat{Q}P_{NN})\hat{G} + \cdots]P^p_{\rm tr}P^p_{\rm def}|_{\theta,\varepsilon}, \tag{4}$$

where the processes are in time order from left to right. $\hat{G}$ is the space development operator for energetic particles, which travel linearly inside the target nucleus. The proton deflection function $P^p_{\rm def}$ is determined to reproduce the angular distribution of elastic scattering, and it provides a deflection angle at the nuclear surface for both the entrance and the exit channels. P_{CE} is the probability of energy transfer by collective excitations. P_{NN} is the NN collision probability to fulfill Eq. (1) and provides the energy and direction of the scattered nucleon after in-medium collision. $P_{\rm tr}$ is the barrier transmission probability for the escaping proton. The functions regarding proton emission are curtailed. After the cascade process, we calculate evaporation using the generalized evaporation model [35].

B. Deuteron production process

We assume that direct pickup and knockout take place via the initial-state interaction with probabilities $P_{\rm dp}$ and $P_{\rm ko}$, respectively. These probabilities are determined to fit experimental data. As Eq. (4), we write the deuteron emission probability by proton bombardment as

$$P^d(\theta,\varepsilon) = P^p_{\rm def}(P_{\rm dp} + \hat{Q}_{p+d}P_{\rm ko})[\hat{G} + \hat{G}(\hat{Q}_{d+N}P_{dN})\hat{G} + \hat{G}(\hat{Q}_{d+N}P_{dN})\hat{G}(\hat{Q}_{d+N}P_{dN})\hat{G} + \cdots]P^d_{\rm tr}P^d_{\rm def}|_{\theta,\varepsilon}, \tag{5}$$

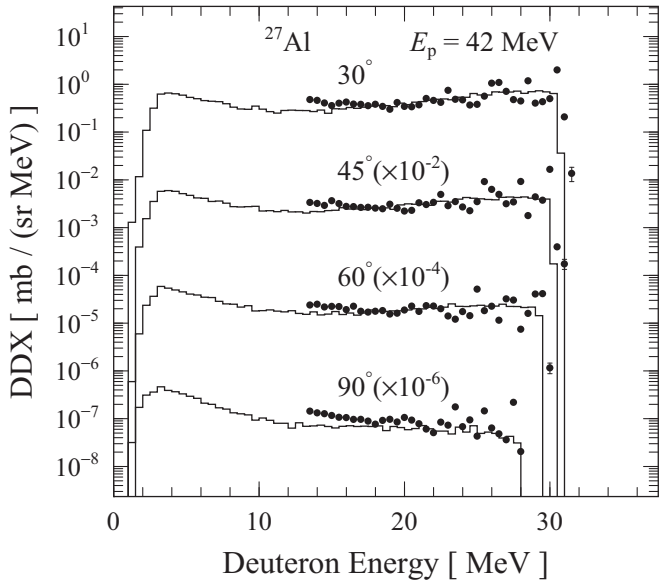

FIG. 1. Spectra of 42-MeV ^{27}Al(p,dx) reactions at 30–90°. Lines and dots show results of present model and experiment, respectively. To avoid overlap, factors indicated in the figure are multiplied.

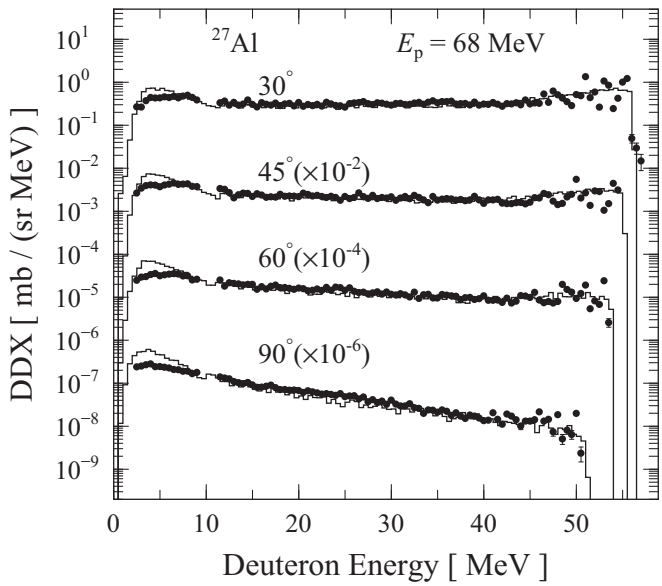

FIG. 2. As Fig. 1 but for 68 MeV.

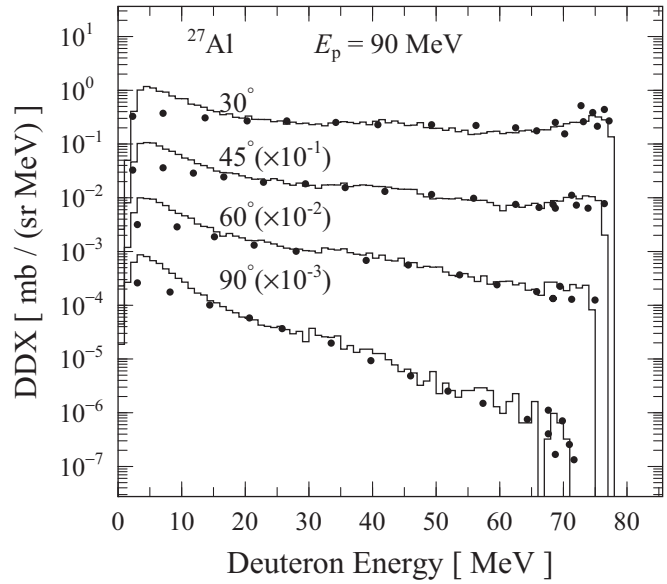

FIG. 3. As Fig. 1 but for 90 MeV.

where $P_{\rm tr}^d$ is the deuteron transmission probability, which is given by the unit step function at the Coulomb potential at a distance of $R_0 + 1.5$ fm from the center of the target nucleus. $\hat{Q}_{p+d}$ is the Pauli blocking operator defined by Eq. (2) for in-medium $p + d$ collision, and P_{dN} is the deuteron-nucleon collision during deuteron transport inside the nucleus. Herein, we assume that in-medium deuteron-nucleon collision occurs via interaction between a nucleon and one of the nucleons of the deuteron. The deuteron deflection $P_{\rm def}^d$ is [36]

$$P_{\rm def}^d(\theta) = \exp\left[-0.001(1.3\varepsilon + \ln A + 6)\theta\right] \tag{6}$$

in terms of ε and target mass A. Assuming that the maximum single-hole excitation is the 45-MeV depth of the nuclear potential, we write $P_{\rm dp}$ as

$$P_{\rm dp} = N \int_0^{45} W_{\rm dp}(U) dU, \tag{7}$$

where N is the normalization factor and $W_{\rm dp}(U)$ is a strength distribution function with excitation energy U:

$$W_{\rm dp}(U) = s(U)\rho(U) + \frac{\Gamma^2}{U^2 + \Gamma^2}. \tag{8}$$

The state density $\rho(U)$ is formulated [37] by

$$\rho(U) = \frac{(U - 0.25(p^2 + h^2 + p - 3h))^{p+h-1}}{p!\, h!(p + h - 1)!} \tag{9}$$

for the excited states of p particles and h holes. In this case, we used $p = 0$ and $h = 1$. $s(U)$ is introduced to dampen transition strength to highly excited states and limit the maximum single-hole excitation:

$$s(U) = \begin{cases} 1 & : 0 < U < 35 \\ 0.05(55 - U) & : 35 \leqslant U < 45. \end{cases} \tag{10}$$

The second term of Eq. (8) expresses the high susceptibility of strong transitions to low-excitation states, among which the strength distribution is well described by the Breit-Wigner function. We choose the width Γ as 10 MeV from results of Refs. [3–5]. We note that in Ref. [33] the single-particle energy of a picked-up neutron was calculated from its in-medium momentum assigned as the initial value of the INC nuclear ground state under the on-shell condition. However, momentum is not an eigenvalue in the nuclear system, and this implementation is less reasonable for light and heavy nuclei. Therefore, we determine the excitation energy of the single-hole state independently herein.

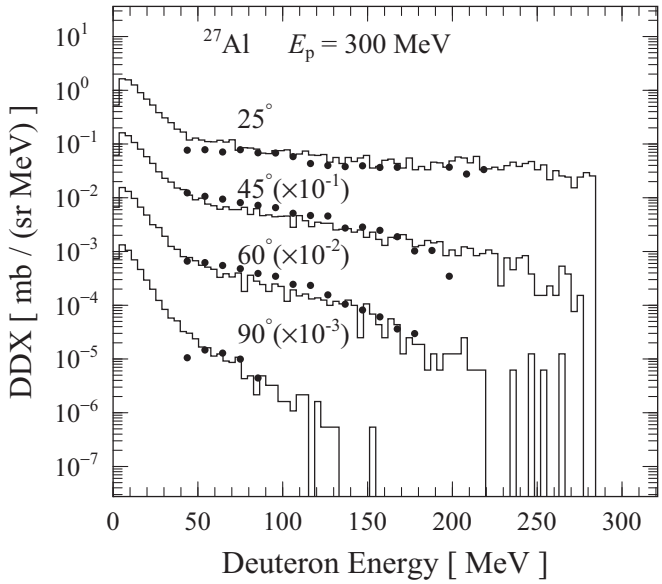

FIG. 4. As Fig. 1 but for 300 MeV.

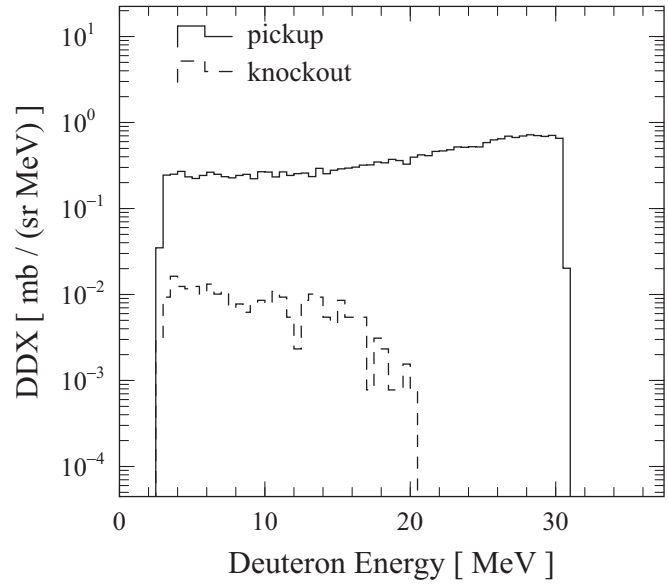

FIG. 6. Contributions of direct pickup (solid line) and knockout (broken line) for 42-MeV ^{27}Al(p,dx) at 30°.

The kinetic energy of a deuteron produced by direct pickup is given by

$$\varepsilon_d = E_{\rm inc} - U \tag{11}$$

in the nucleus. We take the reaction Q value and the recoil of the residual nucleus into account as a final-state interaction.

For the knockout calculation, the preformed deuteron is prepared at the nuclear surface where the incident proton arrives. As the deuteron constituents, we choose the proton and neutron located closest to the proton arrival position. We then reassign their locations and momenta: The location of one is to be the arrival position, the location of the other is determined randomly within a sphere of deuteron radius, and their momenta are determined so as to correspond to the on-shell single-particle energy given by Eq. (8).

Indirect pickup is also included in the present model, the implementation of which is described in Ref. [29]. When a cascade nucleon i is escaping the target nucleus, it can pick up another nucleon j having the opposite iso-spin under the condition

$$r_{ij}\, p_{ij} \leqslant \lambda, \tag{12}$$

where r_{ij} and p_{ij} are the relative position and momentum, respectively, of particles i and j. λ is the clustering parameter determined in Ref. [29].

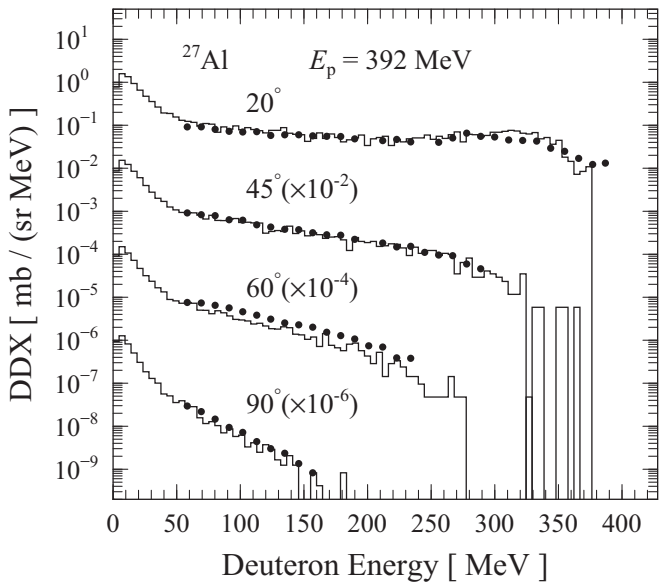

FIG. 5. As Fig. 1 but for 392 MeV.

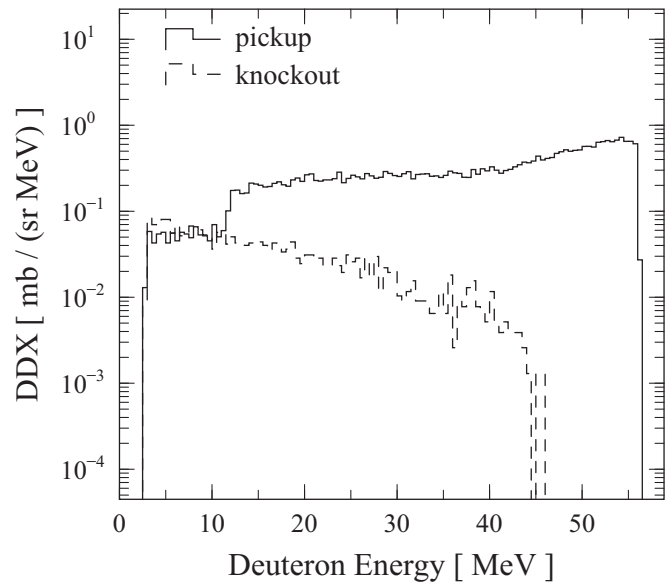

FIG. 7. As Fig. 6 but for incident energy of 68 MeV.

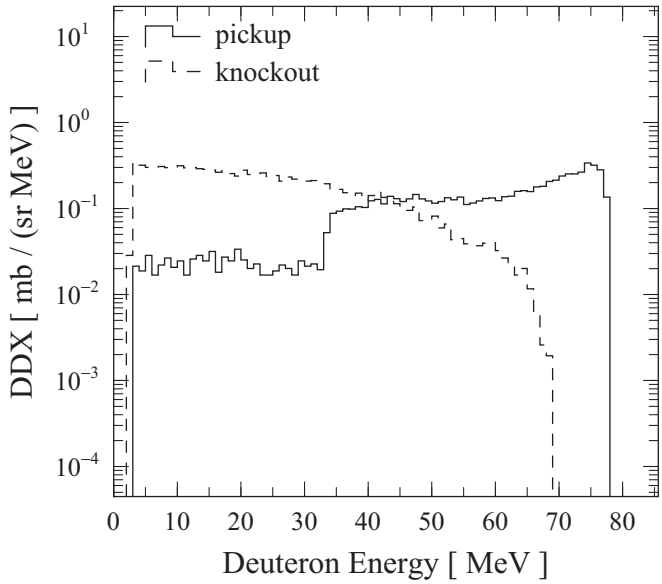

FIG. 8. As Fig. 6 but for incident energy of 90 MeV.

III. RESULTS AND DISCUSSION

The spectral DDXs for ^{27}Al(p,dx) reactions as obtained from calculations (solid lines) and experiments (dots) are displayed in Figs. 1–3 at incident energies of 42, 68, and 90 MeV, respectively. The measured laboratory angles are indicated in the figures. The experiments at 42 and 68 MeV were carried out by Harada *et al.* [38], and those at 90 MeV were carried out by Wu *et al.* [39]. The numerical data are cited from Ref. [40]. The calculation results agree well with the experimental data at all angles and over the entire energy range except in the evaporation region. At the highest energies in the forward-angle spectra, the scatter in the experimental data is due largely to several strong transitions to low-lying discrete levels. The second term of Eq. (8) is responsible for this energy domain and is found to reproduce reasonably the average trend of the experimental data. In Figs. 4 and 5, the calculation results for the 300- and 392-MeV reactions, respectively, are compared with the experimental data [29]. Taking into consideration the lack of experimental data above 200 MeV for the 300-MeV reaction, we conclude that the present model gives fair accounts at these energies. We note that the quasi-free-like bump observed at 20° in the 392-MeV reaction is reproduced well by the calculation. By contrast, calculation with the previous model underestimated the experimental data considerably at large angles [29]. The essential improvement in this regard must be the inclusion of particle deflections at both the entrance and exit channels.

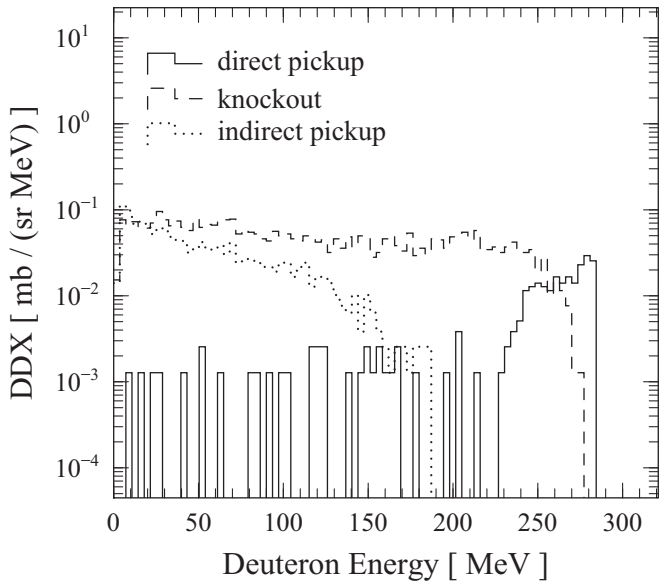

FIG. 9. Contributions of direct pickup (solid line), knockout (broken line), and indirect pickup (dash-dotted line) for 300-MeV ^{27}Al(p,dx) at 20°.

The contributions of pickup and knockout are shown by the solid and broken lines, respectively, in Figs. 6–8 for incident energies 42, 68, and 90 MeV, respectively. The evaporation yields are not displayed. Because direct pickup occupies the entire range at 42 MeV, knockout is assumed to be small enough. As shown in Fig. 7 at 68 MeV, the knockout yield increases from that in the case of 42-MeV incidence, but direct pickup is still dominant down to around 12 MeV, which corresponds to an excitation of roughly 45 MeV. The knockout yield is comparable to the rescattering yield of the direct pickup observed below roughly 12 MeV, where evaporation is dominant. At 90 MeV (Fig. 8), the knockout contribution increases to account for the lower half of the spectrum, and its total yield is comparable with that of direct pickup. For the 300-MeV case, the components of direct pickup, knockout, and indirect pickup are indicated in Fig. 9 by solid, broken, and dash-dotted lines, respectively. The knockout contribution appears to be dominant over most of the energy range. The direct-pickup contribution is limited to a very narrow region at the highest energies. Unlike at lower incident energies, the indirect-pickup component appears. However, its contribution is still negligible, as suggested in Ref. [27].

The determined values of the model parameters $P_{\rm dp}$ and $P_{\rm ko}$ are listed in Table I as a function of incident energy. The actual knockout probability $\hat{Q}_{p+d}P_{\rm ko}$ (i.e., knockout is allowed by the Pauli principle) is also shown in the third column of Table I. The pickup probability $P_{\rm dp}$ decreases rapidly with increasing incident energy, which is qualitatively consistent with the conclusions of Refs. [28,41]. Meanwhile,

TABLE I. Determined values of probabilities for direct pickup ($P_{\rm dp}$) and knockout ($P_{\rm ko}$), together with actual knockout probability $\hat{Q}_{p+d}P_{\rm ko}$.

	Beam energy	Pickup	Knockout	
	(MeV)	$P_{\rm dp}$ (%)	$P_{\rm ko}$ (%)	$\hat{Q}_{p+d}P_{\rm ko}$ (%)
Al(p,dx)	42	6	$\leqslant$1	$\leqslant$0.4
	68	6	3	1.3
	90	2.5	16	8.5
	300	0.2	7	5.1
	392	0.04	10	7.5

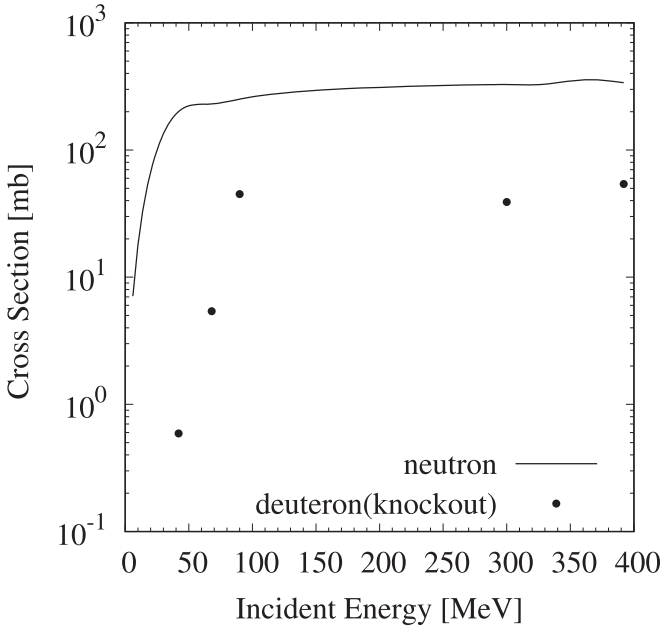

FIG. 10. Cross sections of knockout production for deuterons (dots) and neutrons (solid line) as function of incident proton energy.

the knockout probability increases with incident energy up to 90 MeV and then remains effectively constant for 90–392 MeV. The energy value of 90 MeV is close to the deuteron potential depth. In Fig. 10, we plot deuteron knockout cross sections as a function of incident proton energy. Because we attribute the (p,nx) reaction to the knockout mechanism, we draw its cross section as a solid line in the figure. Both neutron production and deuteron production show similar energy dependences, supporting the deuteron-knockout probability obtained in the analysis with the present model. The neutron cross section becomes constant at around 50 MeV, which is close to the neutron potential depth. This fact is also consistent with the deuteron-knockout case. Therefore, the increasing cross sections with energy can be attributed to the expansion of the final-state phase space.

IV. CONCLUSION

To elucidate the deuteron production mechanism in (p,dx) reactions below 392 MeV, we modeled the processes of direct pickup and knockout and incorporated them into the INC model. Calculations following the evaporation model successfully explained the DDX continua in terms of both shape and magnitude. Pickup occupies the highest energies of the spectra in both the discrete and continuum regions, whereas knockout is located between the pickup and evaporation regions. The contribution of knockout is negligible at 42 MeV, increases to be comparable with that of pickup at 90 MeV, and is dominant above 300 MeV. Indirect pickup takes place at 300 and 392 MeV, but its contribution is limited to the lower spectral energies.

[1] R. Serber, Phys. Rev. **72**, 1114 (1947).
[2] M. L. Goldberger, Phys. Rev. **74**, 1269 (1948).
[3] Syafarudin, F. Aramaki, G. Wakabayashi, Y. Uozumi, N. Ikeda, M. Matoba, K. Yamaguchi, T. Sakae, N. Koori, and T. Maki, J. Nucl. Sci. Technol. Supple. **39**, 377 (2002).
[4] S. Hirowatari, Syafarudin, F. Aramaki, A. Nohtomi, G. Wakabayashi, Y. Uozumi, N. Ikeda, M. Matoba, Y. Aoki, K. Hirota, N. Okumura, and T. Joh, Nucl. Phys. A **714**, 3 (2003).
[5] S. A. Sultana, D. Maki, G. Wakabayashi, Y. Uozumi, N. Ikeda, Syafarudin, F. Aramaki, T. Kawaguchi, M. Matoba, and H. M. Sen Gupta, Phys. Rev. C **70**, 034612 (2004).
[6] S. Hashimoto, Y. Iwamoto, T. Sato, K. Niita, A. Boudard, J. Cugnon, J. C. David, S. Leray, and D. Mancusi, Nucl. Instrum. Methods Phys. Res. B **333**, 27 (2014).
[7] C. Kalbach, Z. Phys. A **283**, 401 (1977).
[8] C. Kalbach, Phys. Rev. C **71**, 034606 (2005).
[9] J. J. Griffin, Phys. Rev. Lett. **17**, 478 (1966).
[10] J. J. Griffin, Phys. Lett. B **24**, 5 (1967).
[11] A. Yu. Konobeyev and Yu. A. Korovin, Kerntechnik **61**, 45 (1996).
[12] C. H. M. Broeders and A. Yu. Konobeyev, Kerntechnik **70**, 1 (2005).
[13] H. Machner, Phys. Lett. B **86**, 129 (1979).
[14] F. Hachenberg, H. C. Chiang, and J. Hufner, Phys. Lett. B **97**, 183 (1980).
[15] L. S. Azhgirei, I. K. Vsorov, V. P. Zrelov, M. G. Mescheryakov, B. S. Neganov, and A. F. Shabudin, JETE (Sov. Phys.) **33**, 1185 (1957).
[16] L. S. Azhgirei, Z. Cisek, Z. V. Krumstein, Yu. P. Merekov, Z. Moroz, N. Q. Zui, V. I. Petrukhin, A. I. Ronzhin, G. A. Shelkov, and O. D. Dalkarov, Nucl. Phys. A **195**, 581 (1972).
[17] R. G. Sutter, J. L. Friedes, H. Palevsky, G. W. Bennet, G. J. Igo, W. D. Simpson, G. C. Phillips, D. M. Corlay, N. S. Wall, and R. L. Stearns, Phys. Rev. Lett. **19**, 1189 (1967).
[18] V. I. Komarov, G. E. Kosarev, E. S. Kuzmin, A. G. Molokanov, G. P. Reshetnikov, O. V. Savchenko, and S. Tesch, Nucl. Phys. A **256**, 362 (1976).
[19] P. C. Gugelot and S. M. Paul, Z. Phys. A **344**, 325 (1993).
[20] S. T. Butler and C. A. Pearson, Phys. Rev. **129**, 836 (1962).
[21] R. K. Shivpuri and B. Bhowmik, Phys. Rev. **186**, 1200 (1969).
[22] D. H. Boal, Phys. Rev. C **25**, 3068 (1982).
[23] J. M. Alexander, D. Guerreau, and L. C. Vaz, Z. Phys. A **305**, 313 (1982).
[24] V. B. Gavrilov, N. L. Kornienko, G. A. Leksin, and S. V. Semenov, Z. Phys. A **324**, 75 (1986).
[25] M. Buscher, A. A. Sibirtsev, and K. Sistemich, Z. Phys. A **350**, 161 (1994).
[26] K. Tokushuku, H. Enyo, T. Nagae, H. Sano, S. Sasaki, M. Sekimoto, R. Chiba, K. Ichimura, T. Mori, I. Arai, J. Chiba, and K. Nakai, Phys. Lett. B **235**, 245 (1990).
[27] B. H. Bransden, Proc. Phys. Soc. A **65**, 738 (1952).
[28] W. N. Hess and B. J. Moyer, Phys. Rev. **101**, 337 (1956).
[29] Y. Uozumi, Y. Sawada, A. Mzhavia, S. Nogamine, H. Iwamoto, T. Kin, S. Hohara, G. Wakabayashi, and M. Nakano, Phys. Rev. C **84**, 064617 (2011).

[30] R. D. Edge and H. H. Knox, Phys. Rev. **184**, 1034 (1969).
[31] Y. Uozumi, T. Yamada, S. Nogamine, and M. Nakano, Phys. Rev. C **86**, 034610 (2012).
[32] Y. Uozumi, T. Yamada, and M. Nakano, J. Nucl. Sci. Technol. **52**, 264 (2015).
[33] Y. Uozumi, T. Mori, A. Sonoda, and M. Nakano, EPJ Web Conf. **122**, 04001 (2016).
[34] J. Cugnon, D. L'Hote, and J. Vandermeulen, Nucl. Inst. Meth. Phys. Res. B **111**, 215 (1996).
[35] S. Furihata, Nucl. Inst. Meth. Phys. Res. B **171**, 251 (2000).
[36] M. J. Kobra, G. Watanabe, Y. Yamaguchi, Y. Uozumi, and M. Nakano, J. Nucl. Sci. Technol. (online), **55**, 209 (2018).
[37] F. C. Williams, Nucl. Phys. A **166**, 231 (1971).
[38] M. Harada, Y. Watanabe, Y. Tanaka, Y. Matsuoka, K. Shin, S. Meigo, H. Nakashima, H. Takada, T. Sasa, O. Iwamoto *et al.*, J. Nucl. Sci. Technol. Supple. **39**, 393 (2002).
[39] J. R. Wu, C. C. Chang, and H. D. Holmgren, Phys. Rev. C **19**, 698 (1979).
[40] EXFOR/CSISRS Experimental Nuclear Reaction Data, http://www.nndc.bnl.gov/exfor/exfor00.htm
[41] J. Heidmann, Phys. Rev. **80**, 171 (1950).